Research Article | Vol. 15, No. 1 / 1 Jan 2024 / Biomedical Optics Express 14
Biomedical Optics EXPRESS

Simultaneous detection of urea and lactate in sweat based on a wearable sweat biosensor

HAIFAN YANG,[1,†] YANGYANG JI,[2,†] KANG SHEN,[1] YAYUN QIAN,[1,4] AND CHENCHEN YE[3,5]

[1]Institute of Translational Medicine, Medical College, Yangzhou University, Yangzhou, 225001, China
[2]Department of Science and Education, Traditional Chinese Medicine Hospital of Tongzhou District, Nantong, 226300, China
[3]Department of Science and Education, Yixing Traditional Chinese Medicine Hospital, Wuxi, 214200, China
[4]yyqian@yzu.edu.cn
[5]jsyxycc@126.com
[†]The authors contributed equally to this work

Abstract: Urea and lactate are biomarkers in sweat that is closely associated with human health. This study introduces portable, rapid, sensitive, stable, and high-throughput wearable sweat biosensors utilizing Au-Ag nanoshuttles (Au-Ag NSs) for the simultaneous detection of sweat urea and lactate. The Au-Ag NSs arrays within the biosensor's microfluidic cavity provide a substantial surface-enhanced Raman scattering (SERS) enhancement effect. The limit of detection (LOD) for urea and lactate are 2.35×10^{-6} and 8.66×10^{-7} mol/L, respectively. This wearable sweat biosensor demonstrates high resistance to compression bending, repeatability, and stability and can be securely attached to various body parts. Real-time sweat analysis of volunteers wearing the biosensors during exercise demonstrated the method's practicality. This wearable sweat biosensor holds significant potential for monitoring sweat dynamics and serves as a valuable tool for assessing bioinformation in sweat.

1. Introduction

The analysis of biomarkers in sweat, including metabolites, proteins, and micronutrients, offers critical insights into an individual's health status. It is valuable for the early detection, monitoring, and treatment of various diseases [1]. Urea and lactate, metabolic byproducts of protein and sugar respectively [2], are significant in this context. Typically, lactate concentration in human sweat ranges from 4-25 mmol/L [3]. Produced under anaerobic conditions, lactate concentration escalates when the body fails to efficiently eliminate it [4,5]. Consequently, prolonged exercise can cause lactate accumulation in muscles, making lactate levels a vital metric for monitoring training [6]. Similarly, the urea content in sweat correlates with blood urea levels, with the normal concentration in human sweat being approximately 20 mmol/L. Sweat urea is crucial for diagnosing kidney and renal dysfunctions [7]. Thus, simultaneous detection of urea and lactate in sweat offers preliminary insights into human metabolism and nutritional health [8,9]. Traditional sweat tests involve separate procedures for sampling and analysis, requiring complex collection processes and specialized personnel. Results are typically processed in a laboratory, precluding real-time monitoring [10–13]. Consequently, portable devices that integrated sweat collection and analysis present a significant market opportunity.

Wearable sweat biosensors are increasingly recognized as an effective alternative to complex interferometry and monitoring techniques [14,15]. Their affordability, simplicity, and ease of use make them vital for human health monitoring [16–18]. These systems usually employ epidermal paper/microfluidic platforms to collect and channel sweat to a sensor [19]. Although they are lightweight, flexible, and cost-effective, they are prone to damage during movement

#505004 https://doi.org/10.1364/BOE.505004
Journal © 2024 Received 5 Sep 2023; revised 19 Nov 2023; accepted 19 Nov 2023; published 4 Dec 2023

Biomedical Optics EXPRESS

and can easily accumulate grease and other contaminants, complicating maintenance. Sweat analysis has employed various methods, including colorimetric [20], fluorescence [21], and electrochemical detection [22,23]. Colorimetric methods, however, rely heavily on the stability of reagents, with factors like temperature, pH, and humidity affecting results [24]. Fluorescence methods, while less susceptible to ambient light interference, depend more on optical modules [25]. Electrochemical methods can detect only one substance and require an energy source, making them bulky and complex [26]. Therefore, there is a pressing need to develop a durable, accurate, stable, and straightforward method for real-time sweat biomarker detection.

Surface-enhanced Raman scattering (SERS) is extensively utilized for detecting various pathogens and biomarkers, owing to its excellent photostability, exceptionally high sensitivity, and rapid readout capabilities [27–29]. The amplification in SERS is primarily dependent on the size, shape, and elemental composition of noble metal nanomaterials [30,31]. Specifically, Au-Ag nanoshuttles (Au-Ag NSs), featuring Au nanorods (Au NRs) as the core and a higher surface concentration of Ag, which grows epitaxially to form sharp tips, have been employed for enhanced SERS detection [32,33]. Au-Ag NSs exhibit significant electromagnetic (EM) field enhancement and large extinction cross-sections, yielding a strong plasmonic response and mediation ability. Consequently, Au-Ag NSs are promising candidates for SERS-based technological applications. A high-performance SERS substrate is crucial for the efficacy of SERS technology. The Au-Ag NSs have been organized into an orderly SERS substrate through self-assembly at the oil-water interface, achieving uniform distribution of high-density SERS "hotspots" and providing significant SERS enhancement [34]. This arrangement also ensures excellent signal uniformity and reproducibility, thereby guaranteeing data reliability [35,36], making the Au-Ag NSs substrate a potential candidate for SERS assays.

Despite its advantages, SERS technology faces challenges due to time-consuming and complex processes [37]. The integration of SERS with wearable technologies to create flexible plasmonic devices has garnered significant interest for various biomedical applications. Microfluidic chips, also known as lab-on-chip (LOC) [38], consolidate essential operations like sample processing, reaction, separation, and detection. They manage sample flow and mixing within microchannels for efficient processing and analysis [39,40]. The comb structure in sweat biosensors drives liquid flow without external pumps and minimizes mixing of old and new sweat, ensuring refreshed SERS assays [41,42]. Therefore, combining microfluidic chips with SERS technology enables real-time collection, storage, and SERS analysis of sweat.

This study developed wearable sweat biosensors capable of highly sensitive, rapid, and high-throughput simultaneous detection of urea and lactate in sweat by merging microfluidic and SERS technologies. Initially, Au-Ag NSs were synthesized using the seed growth method and later organized into arrays via self-assembly at the n-hexane/water (oil-water) interface. The performance of the fabricated wearable sweat biosensors, including their stability, reproducibility, and sensitivity, was rigorously evaluated. These biosensors were then utilized to analyze the sweat of volunteers for urea and lactate content. The wearable sweat biosensor based method for the detection of urea and lactate in swear is shown in Fig. 1. In summary, this sensor provides users with valuable insights into their body's metabolism and health status, enhancing their understanding of personal health.

Biomedical Optics EXPRESS

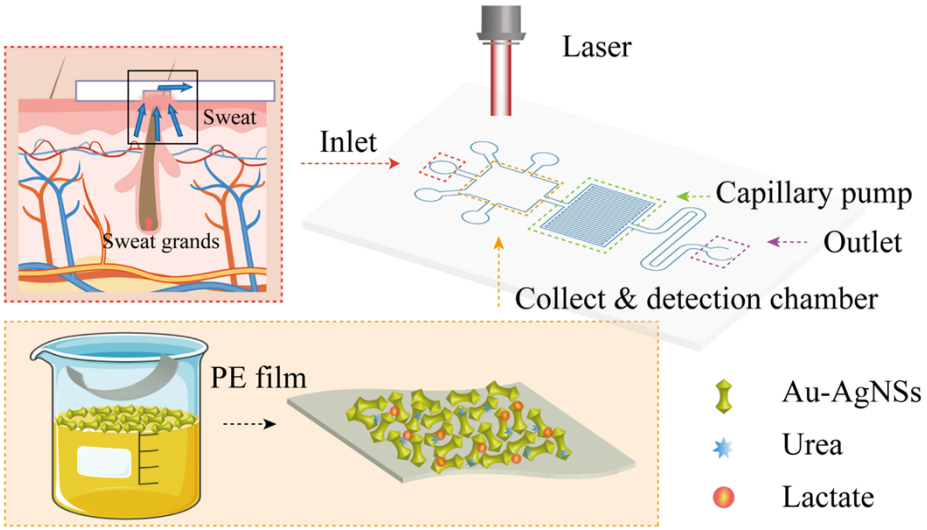

Fig. 1. Schematic diagram of wearable sweat biosensors.

2. Experimental section

2.1. Materials

Chloroauric acid tetrahydrate ($HAuCl_4$), ascorbic acid (AA), sodium oleate (NaOL), sodium borohydride ($NaBH_4$), hydrochloric acid (HCl), absolute ethanol, and hexadecyl trimethyl ammonium bromide (CTAB) were procured from Nanjing Chemical Reagent Co. Ltd. 4-Mercaptobenzoic acid (4-MBA), n-hexane, silver nitrate ($AgNO_3$) were sourced from Suzhou Suyuan Chemical Reagent Co. Ltd. PE film and cling film were obtained from Nantong Ruihuo Experimental Equipment Co., while Polydimethylsiloxane (PDMS) (Dow Corning DC184) was purchased from Sigma-Aldrich. Deionized water used for sample preparation was purified by a Milli-Q system (resistivity of 18.2 MΩ cm).

2.2. Synthesis of Au-Ag NSs

The synthesis of Au-Ag NSs commenced with the preparation of Au NRs. Initially, a freshly prepared $NaBH_4$ solution (0.6 mL, 10 mmol/L) was refrigerated at 4°C. A mixture of CTAB (9.9 mL, 0.1 mol/L) and $HAuCl_4$ (0.1 mL, 25 mmol/L) solutions was then prepared, followed by the addition of 0.6 mL $NaBH_4$ solution. After stirring (700 rpm, 2 min), the solution was aged for 2 h at 30°C to yield the Au seed solution. Subsequently, 1.44 mL, 10 mmol/L $AgNO_3$ solution, and 2 mL, 25 mmol/L $HAuCl_4$ solution were added to 100 mL of a solution mixed with 0.37 mol/L CTAB solution and 0.078 mol/L NaOL. The mixed solution was stirred at 700 rpm, 30°C for 90 min. Thereafter, 0.42 mL hydrochloric acid (37%) and 0.16 mL freshly prepared AA (0.1 mol/L) were introduced, followed by stirring for 5 min. Finally, 0.08 mL of the Au seed solution was added and stirred gently at 30°C for 12 h to complete the Au NRs growth.

To proceed, 5 mL of the final product from the previous step was taken, and 0.091 g CTAB, 5 mL AA solution (0.2 mol/L), and 30 mL NaOH solution (2 mol/L) were sequentially added. Then, 40 mL $HAuCl_4$ solution (25 mmol/L), 0.2 mL $AgNO_3$ solution (10 mmol/L), and 0.2 mL AA solution (0.1 mol/L) were incorporated with vigorous stirring. After stirring for 30 s, the reaction mixture was aged for 1 h to complete the synthesis of Au-Ag NSs. The mixture was then centrifuged (7500 rpm, 10 min) to remove excess reactants and the Au-Ag NSs were redispersed in ultrapure water and stored at 4°C.

Biomedical Optics EXPRESS

2.3. Preparation of Au-Ag NSs SERS arrays

Initially, 3 mL of the Au-Ag NSs solution and 6 mL of n-hexane were combined in a 20 mL beaker and stirred for 3 min. Anhydrous ethanol was then added dropwise to facilitate the formation of Au-Ag NSs arrays. Upon the formation of a monolayer, a flexible transparent PE film was employed to retrieve the Au-Ag NSs monolayer, which was then air-dried at room temperature. The dried film was cut into 4×4 mm squares for storage.

2.4. Fabrication of the wearable sweat biosensors

The wearable sweat biosensor was initially designed using AutoCAD software and a PDMS microfluidic mold was prepared via soft lithography [43]. PDMS adhesive A and B were mixed in a 10:1 mass ratio, vacuum-degassed, poured over the prepared template, and cured in a constant temperature oven at 85°C for 20 min. After cooling to room temperature, the PDMS was carefully peeled off (to avoid damaging the silicon wafer) and then cut and punched to form the PDMS channel layer and outlet layer. Finally, these layers were baked in an 85°C constant temperature oven for 2 hours to complete the wearable sweat biosensor [44].

2.5. Hydrophilic treatment

To facilitate sweat flow within the biosensor, the sensor surface underwent hydrophilic treatment using a PEG polymer coating [45]. Initially, the PDMS layer was cleaned with isopropanol for 5 minutes, followed by drying. The biosensor was then subjected to oxygen plasma treatment for 90 s, after which the PEG-coated biosensor was heated on a hot plate at 150°C for 30 minutes. The final step involved washing the biosensor five times with isopropanol and deionized water, sequentially, and then storing it at 4°C for one hour. This procedure completed the hydrophilic treatment process.

2.6. SERS measurement

SERS spectra were primarily obtained using a portable Raman spectrometer. The measurement settings included an optical power of 200 mW and an integration time of 15 s. To assess the uniformity of the substrates, SERS mapping was performed with a Renishaw Invia microscope Raman spectrometer at a laser power of 5 mW. The SERS spectra were acquired in the reaction region at a wavelength of 785 nm, using a 50-objective lens, and an exposure time of 10 seconds for all measurements. The scanning area covered was 50×50 μm.

2.7. Data analysis

The limit of detection (LOD) was calculated using the characteristic peaks of the SERS spectra and the equation: $LOD = 10^{\frac{(C_{blank}+3SD)-a}{b}}$, where a and b are constants derived from a linear regression of the signal-concentration curve, SD represents the standard deviation, and C_{blank} is the SERS intensity of the blank sample. Similarly, the limit of quantification (LOQ) was determined using the equation: $LOQ = 10^{\frac{(C_{blank}+10SD)-a}{b}}$, employing the same constants a and b in the LOD calculation.

2.8. Human sweat experiment

Prior to the experiment, the arm's surface was thoroughly cleansed with warm water and soap to remove any dirt and grease. The wearable sweat biosensor was then affixed to the cleaned and dried arm using cling film, ensuring full skin contact to prevent air bubbles. The volunteers engaged in moderate, consistent physical activity to induce sweating. The biosensor on the arm was analyzed using a portable Raman spectrometer at five-minute intervals, starting at the 10th minute, for a total of five times. The collected SERS spectra were subsequently stored and

Biomedical Optics EXPRESS

analyzed, allowing for the determination of composition and concentration changes in the sweat, as indicated by the characteristic peaks and intensities in the spectra.

2.9. Characterization

The structural morphology, composition, and size were characterized using a TECNAI 12 transmission electron microscope (TEM) and a Hitachi S-4800 field-emission scanning electron microscope (SEM). Additionally, a FEI field emission transmission electron microscope, equipped with energy-dispersive X-ray spectroscopy (EDS), was used for high-resolution transmission electron microscopy (HRTEM) analysis. UV-Vis-NIR absorption spectra were measured with an Agilent Cary 60 UV-Vis-NIR spectrometer. Ion chromatography Systems were conducted using the Dionex Integration high-pressure ion chromatography (HPIC) system.

3. Result and discussion

3.1. Characterization of Au-Ag NSs

The synthesized Au-Ag NSs were characterized using SEM (Fig. 2(A)) and TEM (Fig. 2(B)). The Au-Ag NSs displayed uniform shape and structural integrity, with an average length of approximately 120 nm and a width of 30 nm. The HRTEM image (Fig. 2(C)) revealed distinct lattice stripes, with an interplanar spacing of 0.209 nm corresponding to the Au {100} plane. The energy dispersive X-ray (EDX) spectra (Fig. 2(D)) confirmed the presence of Au and Ag atoms, with a predominance of Au. This composition combines the chemical stability of Au nanoparticles with the strong SERS enhancement effect of Ag nanoparticles. Peaks of Cu and C were attributed to the copper grid and other reagents. The UV-Vis-NIR absorption spectra (Fig. 2(E)) of both Au NRs and Au-Ag NSs, formed by surface growth on Au NRs, revealed two plasmon bands. The Au NRs exhibited a weak transverse surface plasmon resonance (TSPR) band at 556 nm and a stronger longitudinal band (LSPR) at 860 nm. In comparison, the Au-Ag NSs showed similar bands, blue-shifted to approximately 503 and 801 nm, likely due to the silver coating [46]. The absorption spectra of the Au-Ag NSs were markedly stronger than those of the Au NRs, indicating enhanced local field strength [47].

3.2. Characterization of Au-Ag NSs arrays

Fig. 3(A) displays the SEM image of the Au-Ag NSs arrays self-assembled at the oil-water interface, forming a typical monolayer of evenly spaced NSs. To assess signal uniformity, SERS mapping was conducted on the Au-Ag NSs using 4-MBA as the probe molecule. The intensity distribution of the SERS signal across the arrays was visualized using a color comparison scheme, transitioning from blue (lowest intensity) to red (highest intensity). The uniform color distribution in Fig. 3(B) indicates significant homogeneity in the Au-Ag NSs arrays. Additionally, SERS intensity at 1078 cm^{-1} was analyzed at fifteen randomly selected detection sites on the arrays' surface (Fig. 3(C)), revealing a relative standard deviation (RSD) of 5.75%. These results demonstrate the arrays' homogeneity, crucial for consistent SERS signals and reliable quantitative analysis. In essence, SERS substrates show immense potential and diverse field applications.

The SERS enhancement effect of the Au-Ag NSs arrays was evaluated in Fig. 3(D). Labeled with 4-MBA, the arrays exhibited a prominent SERS peak at 1078 cm^{-1}, attributable to the aromatic ring's vibration [48]. This peak intensity suggests a significant surface enhancement effect due to the "hot spots" at the ends of the Au-Ag NSs. Furthermore, the orderly arrangement of these hot spots on the highly structured SERS substrate enhances the overall SERS effect. The enhancement factor (EF) for the Au-Ag NSs arrays was calculated with the following formula: $EF = \frac{I_{SERS}/C_{SERS}}{I_{RS}/C_{RS}}$, where C_{SERS} and I_{SERS} are the analyte concentration and SERS intensity at the arrays, respectively, and C_{RS} and I_{RS} are the concentration and intensity in a non-SERS state. With C_{SERS} and C_{RS} of 1×10^{-2} and 1×10^{-7} mol/L, I_{SERS} and I_{RS} of 27334.22 and 216.65 a.u.,

Biomedical Optics EXPRESS

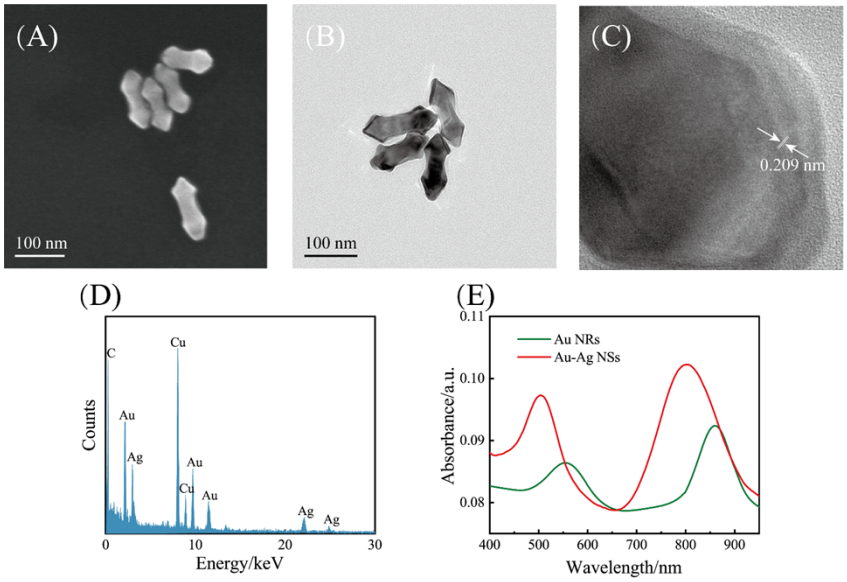

Fig. 2. (A) SEM images, (B) TEM images and (C) HRTEM images of the Au-Ag NSs. (D) EDX spectra and (E) UV-Vis-NIR absorption spectra of the Au NRs and Au-Ag NSs.

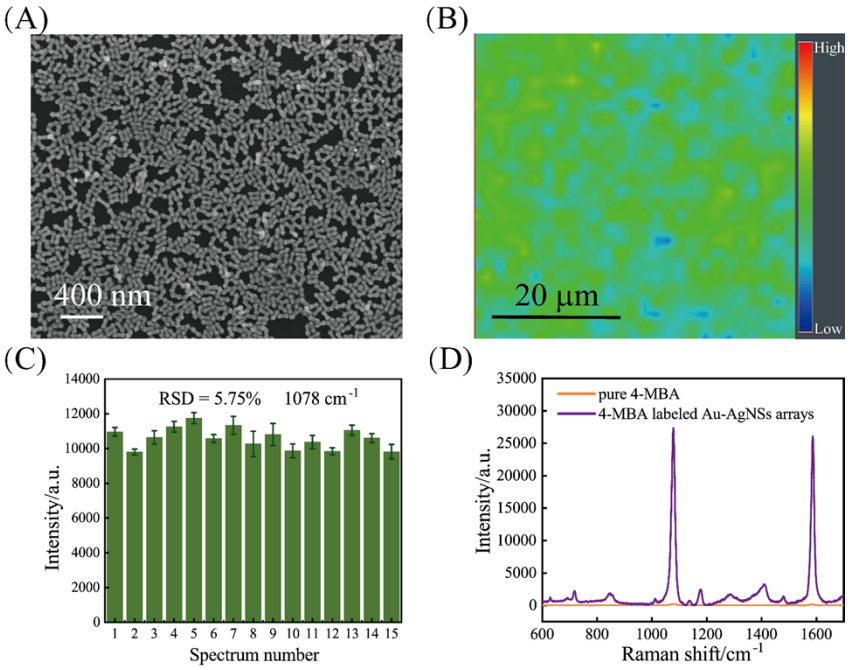

Fig. 3. SEM image of Au-Ag NSs arrays (A). (B) SERS mapping of 4-MBA labelled Au-Ag NSs arrays. (C) Fifteen points randomly selected on the Au-Ag NSs arrays corresponding histogram of SERS intensity at 1078 cm^{-1}. (D) SERS spectra of pure 4-MBA, 4-MBA labelled Au-Ag NSs and 4-MBA labelled Au-Ag NSs arrays.

Biomedical Optics EXPRESS

respectively, the EF value of Au-Ag NSs arrays was 1.26×10^8, which was much higher than 3.9×10^7 for gold nanorod substrates [49], highlighting that the Au-Ag NSs arrays' remarkable SERS enhancement effect. This efficiency also implies that these substrates can detect target compounds at much lower concentrations. Overall, SERS substrates offer vast potential and wide-ranging application prospects.

3.3. Structure and characterization of a wearable sweat biosensor

The wearable sweat biosensor, depicted in Fig. 4(A), comprises a PDMS channel layer as its base. This layer is segmented into an inlet region, a detection region, and a shunt region. The inlet region contains five downward-facing holes, each 1.5 mm in diameter. The detection area, with a height of 0.35 mm, includes a double-sided adhesive base to secure the SERS substrate and houses a microfluidic cavity filled with Au-Ag NSs arrays, covering an area of 16 mm^2. The shunt region features a comb-like structure and a liquid outlet, where the channels of the comb are 0.2 mm wide and others are 0.5 mm wide, all maintaining a height of 0.2 mm. The individual PDMS layers have a thickness of 0.5 mm. The outlet comprises a single hole of 1.5 mm in diameter. Detailed dimensions of the biosensor are illustrated in Figs. 4(B) and 4(C). Positioned above the channel layer are the PDMS outlet layer and a cling film layer, each with a perforation hole aligning with the outlet in the PDMS channel layer, facilitating sweat flow. Once sweat enters through the inlet, it smoothly transitions through the microchannel to the Au-Ag NSs arrays for SERS detection.

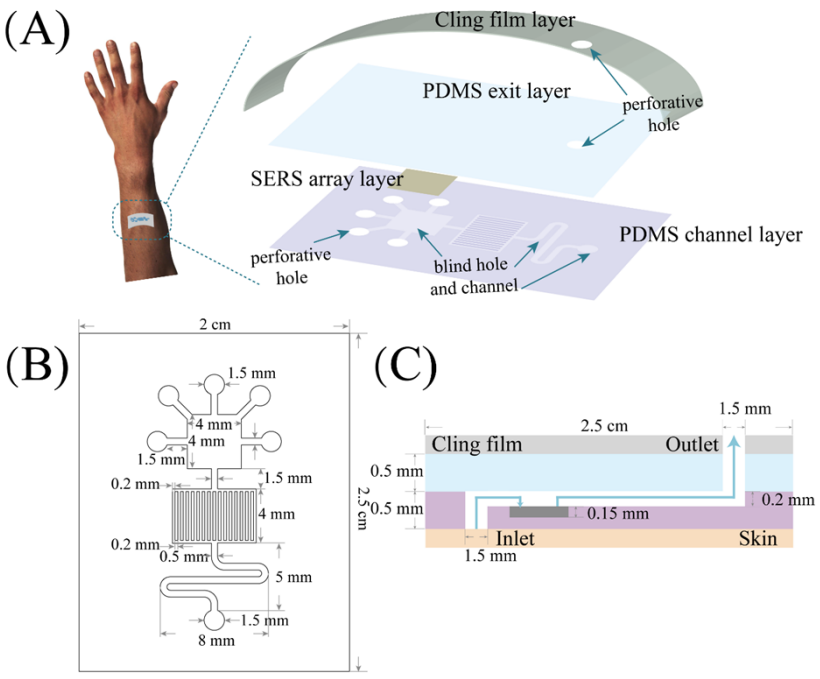

Fig. 4. Structural hierarchy (A) and detailed dimensions (B, C) of the wearable sweat biosensors.

3.4. Performance evaluation of wearable sweat biosensors

The wearable sweat biosensor, fabricated from PDMS, exhibits flexibility and resilience. When subjected to external forces, it deforms but reverts to its original shape upon force removal, as shown in Fig. 5(A), where no permanent deformation occurred under pressure. Further, the

Biomedical Optics EXPRESS

biosensor's SERS signal intensity remained stable under bending conditions, with the ratio of SERS intensity ($I_{bend}/I_{original}$) being nearly consistent, demonstrating the biosensor's stable SERS signal during flexion. As evident in Fig. 5(C), the waveforms of 4-MBA SERS spectra with and without PDMS packing were comparable, displaying characteristic peaks at 1078 cm^{-1}. The SERS signal intensity decreased by only 91.73%, attesting to PDMS's suitability for wearable sweat biosensors.

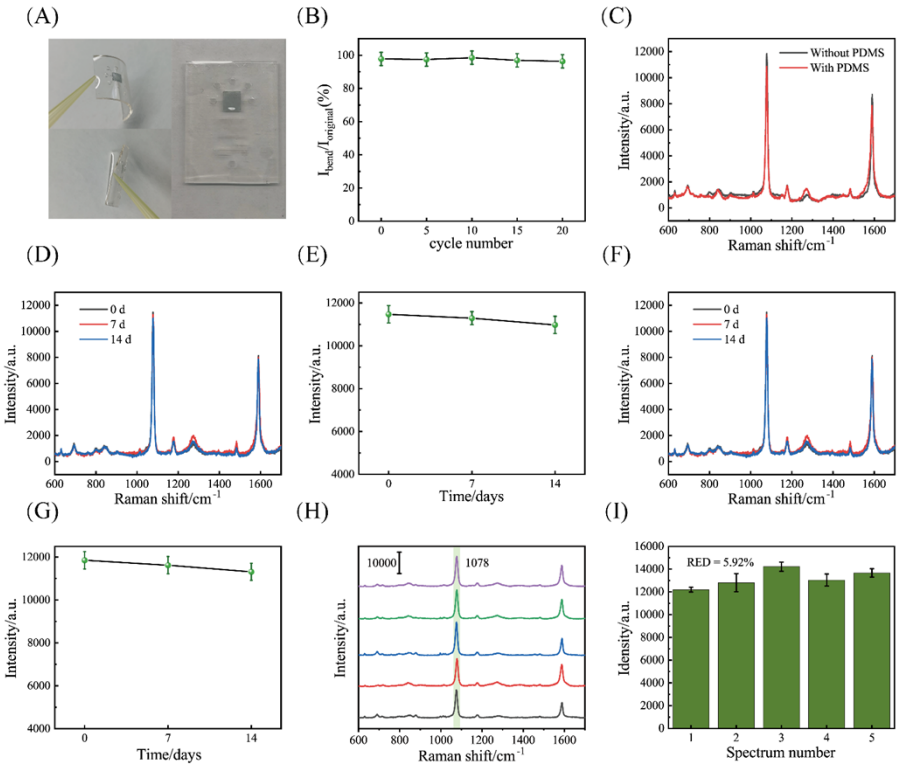

Fig. 5. Physical image of the wearable sweat biosensor under bending (A) and the corresponding intensity changes of the SERS signals (B). Comparison of the SERS signals with and without PDMS package for the detection of 4-MBA. (C) Physical image of the wearable sweat biosensor attached to the human body. (D) SERS spectra of the target 4-MBA using the wearable sweat biosensor stored at 4°C for different times, and (E) corresponding line plot of peak intensities at 1078 cm^{-1}. (F) SERS spectra of target 4-MBA using the wearable sweat biosensor stored at room temperature for different times and (G) corresponding line of peak intensities at 1078 cm^{-1}. (H) SERS spectra of target 4-MBA using the sweat biosensor prepared at different times and (I) corresponding histogram of peak intensities at 1078 cm^{-1}.

To assess the stability of these biosensors, new devices were produced and stored at 4°C and room temperature for 7 and 14 d before SERS detection of 4-MBA. The SERS spectra, as depicted in Fig. 5(D), remained largely consistent across tests, with the SERS intensity at the characteristic peak of 1078 cm^{-1} reducing to 95.67% after 14 d at 4°C (Fig. 5(E)). The biosensor's stability was not significantly impacted at either 4°C or room temperature, with intensity decreases to 95.67% and 95.45%, respectively (Figs. 5(F, G)). This indicates the biosensor's robust stability. Fig. 5(H) shows the SERS spectra of 4-MBA detected by biosensors from different batches, demonstrating consistent characteristic peak locations and intensities. The RSD of 5.92% at

Biomedical Optics EXPRESS

1078 cm^{-1} (Fig. 5(I)) indicates the biosensor's high reproducibility. The device's hermeticity and hydrophilicity were visually confirmed by the flow of red ink.

The biosensor adapts well to the human body's contours and can be affixed to various body parts as needed (Fig. 6(A)). Fig. 6(B) illustrates ink flowing into the microfluidic chamber within 70 s, driven by capillary action, and exiting the outlet after 490 s, without any leakage, confirming the biosensor's effective sealing and hydrophilicity.

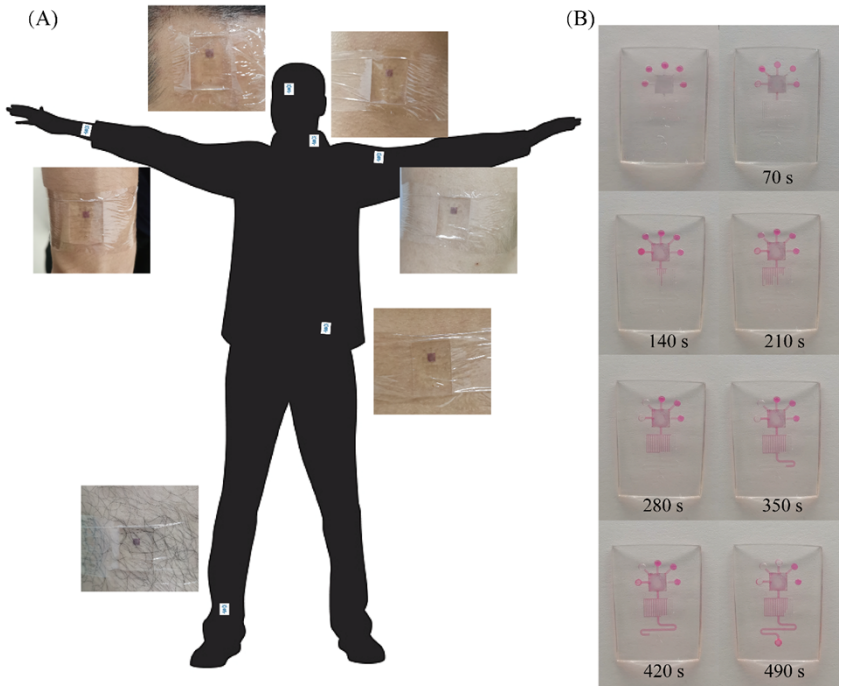

Fig. 6. (A) Physical image of the wearable sweat biosensor affixed to the human body. (B) Digital images of inks automatically flowed in the microfluidic channel by capillary force according to time.

3.5. Quantitative analysis and creation of a standard curve

As illustrated in Fig. 7(A), urea displays a distinct characteristic peak at 1010 cm^{-1}, stemming from the symmetrical C-N stretching in the urea molecule [50]. Fig. 7(B) reveals lactate's characteristic peaks at 869, 983, 1056, and 1242 cm^{-1}. The peak at 1056 cm^{-1}, attributed to the C-CH_3 stretching in lactate [51], was chosen as the characteristic peak for lactate. Given that urea and lactate each have unique characteristic peaks and do not require labeling, their simultaneous detection is feasible. As shown in Fig. 7(C), the concurrent detection of urea and lactate exhibits their distinct characteristic peaks, fulfilling the criteria for simultaneous analysis.

Aqueous solutions of urea and lactate at varying concentrations were subjected to SERS analysis, with results presented in Figs. 8(A) and 8(C). As the concentrations of urea and lactate increased, their corresponding SERS intensities also escalated. A linear standard curve for urea (0 - 1 mol/L) was established with a regression equation of $y = 882.97x + 5147.34$, $R^2 = 0.9879$ (Fig. 8(B)). For lactate (0 - 10^{-1} mol/L), the regression equation was $y = 1043.82x + 6457.17$, $R^2 = 0.9808$ (Fig. 8(D)). The C_{blank} for urea and lactic acid were 127.54 and 101.27 a.u. and the SD values were 16.43 and 9.24 a.u. respectively. Thus, the LOQ for urea was 3.17×10^{-6} mol/L

Biomedical Optics EXPRESS

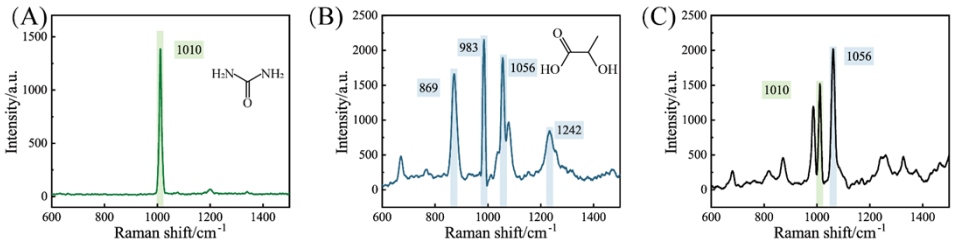

Fig. 7. (A) Urea SERS spectra. (B) Lactate SERS spectra. (C) Urea and lactate simultaneous detection SERS spectra.

and for lactate 9.99×10^{-7} mol/L. Simultaneously, the LOD was 2.35×10^{-6} mol/L for urea and 8.66×10^{-7} mol/L for lactate, underscoring the biosensor's exceptional sensitivity.

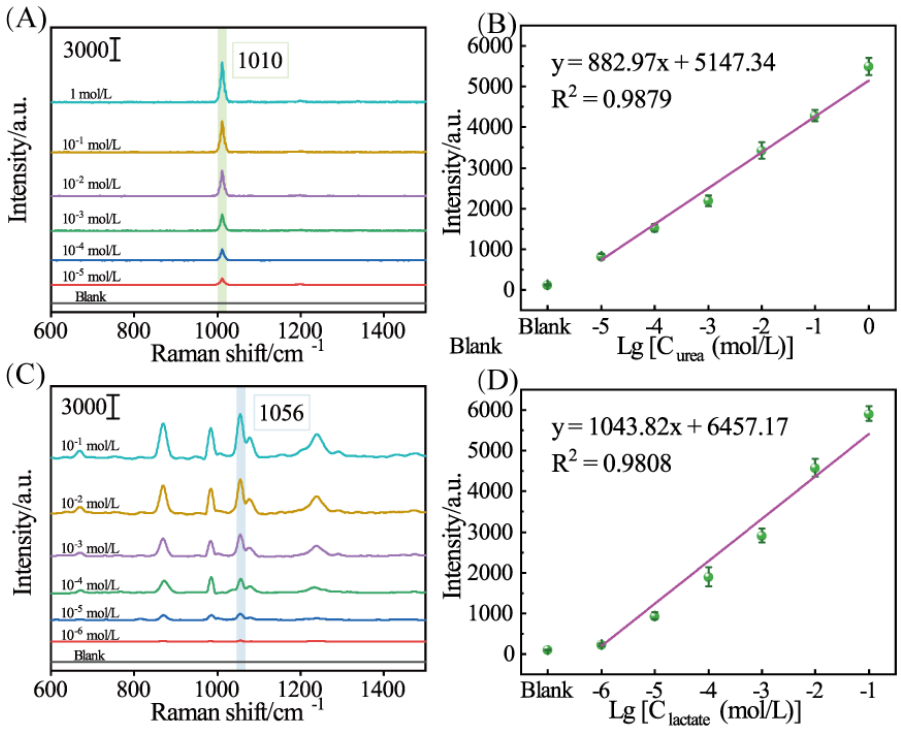

Fig. 8. SERS spectra (A, C) and corresponding linear calibration curves (B, D) for different concentrations of urea and lactate.

When compared with other methods in Table 1, this approach demonstrated lower LODs and a broader detection range. The lower LODs allow the biosensor to detect trace amounts of urea and lactate, enabling more sensitive detection and accurate analysis. Additionally, the wearable sweat biosensor facilitates the simultaneous analysis of both urea and lactate in sweat. This biosensor is user-friendly and suitable for non-invasive, real-time, and continuous monitoring of urea and lactate in sweat.

Biomedical Optics EXPRESS

Table 1. Comparison for determination of urea and lactate using different methods

Analyte	Method	Application	Detection range (mol/L)	LOD (mol/L)	Ref.
Urea	colorimetric	sweat	0 - 2×10^{-2}	5×10^{-5}	[20]
	colorimetric	sweat	0 - 1×10^{-2}	6×10^{-4}	[16]
	Electrochemistry	sweat	10^{-3} - 10^{-1}	1×10^{-4}	[52]
	SERS	sweat	10^{-4} - 1	6.31×10^{-5}	[53]
	SERS	sweat	0 - 1	2.35×10^{-6}	This work
Lactate	colorimetric	sweat	0 - 5×10^{-2}	6.7×10^{-4}	[54]
	Fluorescen	sweat	0 - 10^{-2}	6×10^{-5}	[55]
	Electrochemistry	sweat	3×10^{-3} - 10^{-1}	1.5×10^{-3}	[56]
	SERS and colorimetric	sweat	0 - 10^{-2}	6.9×10^{-5}	[57]
	SERS	sweat	10^{-4} - 4×10^{-2}	5×10^{-5}	[58]
	SERS	sweat	0 - 10^{-1}	8.66×10^{-7}	This work

3.6. *In situ sweat collection and SERS testing*

Fig. 9(A) depicts a male participant wearing a wearable sweat biosensor while engaging in badminton, an activity conducive to sweating in the arms. The sweat analysis, conducted at 5-minute intervals using a portable Raman spectrometer, revealed that urea concentration stabilized at around 20 mmol/L as exercise duration increased. Lactate levels showed a gradual increase during exercise, plateauing between 25-30 min (Fig. 9(C)). These findings, aligning with the established normal range [6,59], suggest the biosensor's efficacy for rapid, non-invasive, and simultaneous monitoring of sweat metabolites. To validate the experimental accuracy, urea and lactate levels were also measured using ion chromatography (HPIC). The comparable results between SERS and HPIC, as presented in Table 2, affirm the biosensor's precision in detecting urea and lactate in real samples.

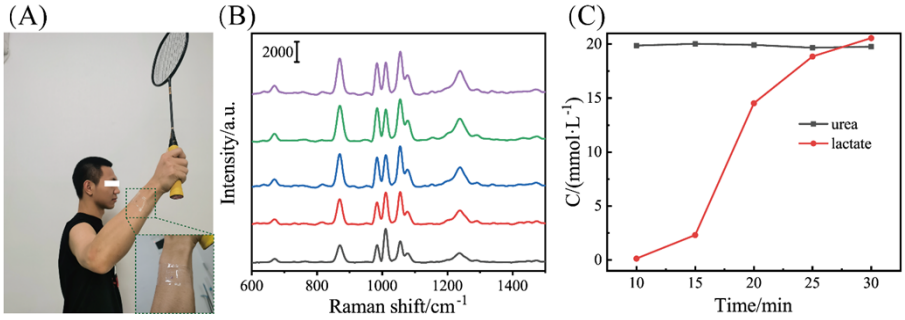

Fig. 9. (A) Images of volunteers wearing the wearable sweat biosensor during exercise. (B) SERS spectra of urea and lactate at varying exercise durations, and (C) calculated levels of the corresponding markers.

Biomedical Optics EXPRESS

Table 2. Comparison of the method proposed in this study with HPIC

Sample	SERS detection (mmol/L)		HPIC (mmol/L)		Relative error (%)	
	Urea	Lactate	Urea	Lactate	Urea	Lactate
1	18.43	13.72	17.64	13.17	4.27	4.01
2	19.07	14.94	18.27	14.39	4.20	3.68
3	18.62	12.56	17.78	12.03	4.51	4.22

4. Conclusion

This study successfully developed a wearable sweat biosensor integrated with Au-Ag NSs arrays, achieving ultrasensitive detection of urea and lactate in sweat. The Au-Ag NSs arrays enhanced SERS amplification, significantly boosting detection sensitivity. The LODs were 2.35×10^{-6} mol/L for urea and 8.66×10^{-7} mol/L for lactate. PDMS, notable for its flexibility and biocompatibility, maintained 91.37% of SERS signal intensity post-packaging, rendering it ideal for wearable biosensor fabrication. The biosensor's multi-channel design expedited sweat entry, while the capillary pump ensured swift filling of the microfluidic chamber within 70 s, enhancing detection efficiency. Linear regression equations for urea and lactate detection were established, with measured concentrations in sweat falling within the normal range, demonstrating the method's viability. The wearable sweat biosensor offers a fast, convenient approach for detecting urea and lactate in sweat. Future work will focus on further optimizing the biosensor to advance sweat detection technology.

Funding. The Social Development Project of Yixing (2021SF15).

Disclosures. The authors declare that there are no conflicts of interest related to this article.

Data availability. Data underlying the results presented in this paper are not publicly available at this time but may be obtained from the authors upon reasonable request.

References

1. Z. Zhao, Q. Li, L. Chen, *et al.*, "A thread/fabric-based band as a flexible and wearable microfluidic device for sweat sensing and monitoring," Lab Chip **21**(5), 916–932 (2021).
2. L. B. Baker, "Physiology of sweat gland function: The roles of sweating and sweat composition in human health," Temperature (Austin) **6**(3), 211–259 (2019).
3. M. M. Pribil, G. U. Laptev, E. E. Karyakina, *et al.*, "Noninvasive hypoxia monitor based on gene-free engineering of lactate oxidase for analysis of undiluted sweat," Anal. Chem. **86**(11), 5215–5219 (2014).
4. P. J. Derbyshire, H. Barr, F. Davis, *et al.*, "Lactate in human sweat: A critical review of research to the present day," J Physiol Sci **62**(6), 429–440 (2012).
5. C.-H. Chen, P.-W. Lee, Y.-H. Tsao, *et al.*, "Utilization of self-powered electrochemical systems: Metallic nanoparticle synthesis and lactate detection," Nano Energy **42**, 241–248 (2017).
6. T. T. Luo, Z. H. Sun, C. X. Li, *et al.*, "Monitor for lactate in perspiration," J Physiol Sci **71**(1), 26 (2021).
7. Y. Zhang, H. Guo, S. B. Kim, *et al.*, "Passive sweat collection and colorimetric analysis of biomarkers relevant to kidney disorders using a soft microfluidic system," Lab Chip **19**(9), 1545–1555 (2019).
8. R. Das, S. Nag, and P. Banerjee, "Electrochemical nanosensors for sensitization of sweat metabolites: From concept mapping to personalized health monitoring," Molecules **28**(3), 1259 (2023).
9. C. F. Greyling, A. Ganguly, A. U. Sardesai, *et al.*, "Passive sweat wearable: A new paradigm in the wearable landscape toward enabling "detect to treat" opportunities," Wiley Interdiscip Rev Nanomed Nanobiotechnol , e1912 (2023).
10. J. Heikenfeld, A. Jajack, J. Rogers, *et al.*, "Wearable sensors: Modalities, challenges, and prospects," Lab on a Chip **18**(2), 217–248 (2018).
11. L. B. Baker, C. T. Ungaro, K. A. Barnes, *et al.*, "Validity and reliability of a field technique for sweat na+ and k+ analysis during exercise in a hot-humid environment," Physiological reports **2**(5), e12007 (2014).
12. M. Ely, B. Ely, T. Chinevere, *et al.*, "Evaluation of the megaduct sweat collector for mineral analysis," Physiol. Meas. **33**(3), 385–394 (2012).
13. A. Mena-Bravo and M. L. De Castro, "Sweat: A sample with limited present applications and promising future in metabolomics," J. Pharm. Biomed. Anal. **90**, 139–147 (2014).
14. M. Dervisevic, M. Alba, B. Prieto-Simon, *et al.*, "Skin in the diagnostics game: Wearable biosensor nano-and microsystems for medical diagnostics," Nano Today **30**, 100828 (2020).

Biomedical Optics EXPRESS

15. S. M. Khor, J. Choi, P. Won, *et al.*, "Challenges and strategies in developing an enzymatic wearable sweat glucose biosensor as a practical point-of-care monitoring tool for type ii diabetes," Nanomaterials (Basel) **12**(2), 221 (2022).
16. X. Yue, F. Xu, L. Zhang, *et al.*, "Simple, skin-attachable, and multifunctional colorimetric sweat sensor," ACS Sens **7**(8), 2198–2208 (2022).
17. L. Chen, F. Chen, G. Liu, *et al.*, "Superhydrophobic functionalized ti(3)c(2)t(x) mxene-based skin-attachable and wearable electrochemical ph sensor for real-time sweat detection," Anal Chem **94**(20), 7319–7328 (2022).
18. V. Myndrul, E. Coy, N. Babayevska, *et al.*, "Mxene nanoflakes decorating zno tetrapods for enhanced performance of skin-attachable stretchable enzymatic electrochemical glucose sensor," Biosens. Bioelectron. **207**, 114141 (2022).
19. J. Yin, J. Li, V. S. Reddy, *et al.*, "Flexible textile-based sweat sensors for wearable applications," Biosensors (Basel) **13**(1), 127 (2023).
20. S. Salatiello, M. Spinelli, C. Cassiano, *et al.*, "Sweat urea bioassay based on degradation of prussian blue as the sensing architecture," Anal Chim Acta **1210**, 339882 (2022).
21. X. Weng, Z. Fu, C. Zhang, *et al.*, "A portable 3d microfluidic origami biosensor for cortisol detection in human sweat," Anal. Chem. **94**(8), 3526–3534 (2022).
22. S. Wang, M. Liu, X. Yang, *et al.*, "An unconventional vertical fluidic-controlled wearable platform for synchronously detecting sweat rate and electrolyte concentration," Biosens. Bioelectron. **210**, 114351 (2022).
23. A. Qureshi and J. H. Niazi, "Graphene-interfaced flexible and stretchable micro-nano electrodes: From fabrication to sweat glucose detection," Mater. Horiz. **10**(5), 1580–1607 (2023).
24. G. G. Morbioli, T. Mazzu-Nascimento, A. M. Stockton, *et al.*, "Technical aspects and challenges of colorimetric detection with microfluidic paper-based analytical devices (μpads) - a review," Anal. Chim. Acta **970**, 1–22 (2017).
25. S. Ye, S. Feng, L. Huang, *et al.*, "Recent progress in wearable biosensors: From healthcare monitoring to sports analytics," Biosensors (Basel) **10**(12), 205 (2020).
26. S. Emaminejad, W. Gao, E. Wu, *et al.*, "Autonomous sweat extraction and analysis applied to cystic fibrosis and glucose monitoring using a fully integrated wearable platform," Proc. Natl. Acad. Sci. U.S.A. **114**(18), 4625–4630 (2017).
27. X. Liu, J. Guo, Y. Li, *et al.*, "SERS substrate fabrication for biochemical sensing: Towards point-of-care diagnostics," J. Mater. Chem. B **9**(40), 8378–8388 (2021).
28. M. J. Oliveira, A. Dalot, E. Fortunato, *et al.*, "Microfluidic sers devices: Brightening the future of bioanalysis," Discov Mater **2**(1), 12 (2022).
29. R. D. Norton, H. T. Phan, S. N. Gibbons, *et al.*, "Quantitative surface-enhanced spectroscopy," Annu. Rev. Phys. Chem. **73**(1), 141–162 (2022).
30. G. M. Das, S. Managò, M. Mangini, *et al.*, "Biosensing using sers active gold nanostructures," Nanomaterials **11**(10), 2679 (2021).
31. X. Li, B. Liu, L. Liu, *et al.*, "Large-scale assembly of geometrically diverse metal nanoparticles-based 3d plasmonic DNA nanostructures for sers detection of pnk in cancer cells," Talanta **266**, 124958 (2024).
32. M. M. Mariscal, J. J. Velázquez-Salazar, and M. J. Yacaman, "Growth mechanism of nanoparticles: Theoretical calculations and experimental results," CrystEngComm **14**(2), 544–549 (2012).
33. G. Awiaz, J. Lin, and A. Wu, "Recent advances of au@ag core-shell sers-based biosensors," Exploration (Beijing) **3**(1), 20220072 (2023).
34. A. Sultangaziyev and R. Bukasov, "Applications of surface-enhanced fluorescence (SEF) spectroscopy in bio-detection and biosensing," Sensing and Bio-Sensing Research **30**, 100382 (2020).
35. M. Cheng, F. Zhang, A. Zhu, *et al.*, "Bridging the neighbor plasma coupling on curved surface array for early hepatocellular carcinoma detection," Sensors and Actuators B: Chemical **309**, 127759 (2020).
36. J. Langer, D. J. de Aberasturi, J. Aizpurua, *et al.*, "Present and future of surface-enhanced raman scattering," ACS nano **14**(1), 28–117 (2020).
37. S. Bock, Y. S. Choi, M. Kim, *et al.*, "Highly sensitive near-infrared sers nanoprobes for in vivo imaging using gold-assembled silica nanoparticles with controllable nanogaps," J Nanobiotechnology **20**(1), 130 (2022).
38. I. J. Jahn, O. Žukovskaja, X. S. Zheng, *et al.*, "Surface-enhanced raman spectroscopy and microfluidic platforms: Challenges, solutions and potential applications," Analyst **142**(7), 1022–1047 (2017).
39. K. Wu, X. He, J. Wang, *et al.*, "Recent progress of microfluidic chips in immunoassay," Front. Bioeng. Biotechnol. **10**, 1112327 (2022).
40. R. Panneerselvam, H. Sadat, E. M. Höhn, *et al.*, "Microfluidics and surface-enhanced raman spectroscopy, a win-win combination?" Lab Chip **22**(4), 665–682 (2022).
41. A. Pradeep, J. Raveendran, and T. G. S. Babu, "Design, fabrication and assembly of lab-on-a-chip and its uses," Prog Mol Biol Transl Sci **187**, 121–162 (2022).
42. E. Samiei, M. Tabrizian, and M. Hoorfar, "A review of digital microfluidics as portable platforms for lab-on a-chip applications," Lab Chip **16**(13), 2376–2396 (2016).
43. D. Qin, Y. Xia, and G. M. Whitesides, "Soft lithography for micro- and nanoscale patterning," Nat Protoc **5**(3), 491–502 (2010).
44. S. Li, Z. Ma, Z. Cao, *et al.*, "Advanced wearable microfluidic sensors for healthcare monitoring," Small **16**(9), 1903822 (2020).
45. P. B. Lillehoj, F. Wei, and C.-M. Ho, "A self-pumping lab-on-a-chip for rapid detection of botulinum toxin," Lab on a Chip **10**(17), 2265–2270 (2010).

Biomedical Optics EXPRESS

46. J. Becker, I. Zins, A. Jakab, *et al.*, "Plasmonic focusing reduces ensemble linewidth of silver-coated gold nanorods," Nano Lett **8**(6), 1719–1723 (2008).
47. T. Bai, J. Sun, R. Che, *et al.*, "Controllable preparation of core–shell au–ag nanoshuttles with improved refractive index sensitivity and sers activity," ACS Appl. Mater. Interfaces **6**(5), 3331–3340 (2014).
48. P. Li, X. Wang, H. Li, *et al.*, "Investigation of charge-transfer between a 4-mercaptobenzoic acid monolayer and tio2 nanoparticles under high pressure using surface-enhanced raman scattering," Chem. Commun. **54**(49), 6280–6283 (2018).
49. Y.-X. Zhao, W.-W. Zhu, Y.-Y. Wu, *et al.*, "Sensitive surface-enhanced raman scattering for the quantitative detection of formaldehyde in foods using gold nanorod substrate," Microchem. J. **160**, 105727 (2021).
50. C. J. Saatkamp, M. L. de Almeida, J. A. M. Bispo, *et al.*, "Quantifying creatinine and urea in human urine through raman spectroscopy aiming at diagnosis of kidney disease," J. Biomed. Opt **21**(3), 037001 (2016).
51. G. Cassanas, M. Morssli, E. Fabregue, *et al.*, "Vibrational spectra of lactic acid and lactates," J. Raman Spectrosc. **22**(7), 409–413 (1991).
52. Y.-L. Liu, R. Liu, Y. Qin, *et al.*, "Flexible electrochemical urea sensor based on surface molecularly imprinted nanotubes for detection of human sweat," Anal. Chem. **90**(21), 13081–13087 (2018).
53. W. Wang, Y. Chen, C. Xiao, *et al.*, "Flexible sers wearable sensor based on nanocomposite hydrogel for detection of metabolites and ph in sweat," Chem. Eng. J. **474**, 145953 (2023).
54. E. Yüzer, V. Doğan, V. Kılıç, *et al.*, "Smartphone embedded deep learning approach for highly accurate and automated colorimetric lactate analysis in sweat," Sensors and Actuators B: Chemical **371**, 132489 (2022).
55. H. D. Duong and J. I. Rhee, "Ratiometric fluorescent biosensors for glucose and lactate using an oxygen-sensing membrane," Biosensors **11**(7), 208 (2021).
56. N. V. Zaryanov, V. N. Nikitina, E. V. Karpova, *et al.*, "Nonenzymatic sensor for lactate detection in human sweat," Anal. Chem. **89**(21), 11198–11202 (2017).
57. U. B. Gunatilake, S. Garcia-Rey, E. Ojeda, *et al.*, "Tio(2) nanotubes alginate hydrogel scaffold for rapid sensing of sweat biomarkers: Lactate and glucose," ACS Appl. Mater. Interfaces **13**(31), 37734–37745 (2021).
58. Z. Zhao, Q. Li, Y. Dong, *et al.*, "Core-shell structured gold nanorods on thread-embroidered fabric-based microfluidic device for ex situ detection of glucose and lactate in sweat," Sensors and Actuators B: Chemical **353**, 131154 (2022).
59. C. T. Huang, M. L. Chen, L. L. Huang, *et al.*, "Uric acid and urea in human sweat," Chin J Physiol **45**, 109–115 (2002).